Towards Knowledge Based Grain Boundary Engineering of Transparent Alumina Combining Advanced TEM and Atomistic Modelling

Abhishek Tewari*[a], Farhang Nabiei[b], Stephen C Parker[c], Marco Cantoni[b], Michael Stuer[a], Paul Bowen[a], and Cécile Hébert[b]

[a] *Laboratory of Powder Technology, Dept. of Materials Science, École Polytechnique Federale de Lausanne, CH-1015, Lausanne, Switzerland.*

[b] *Electron Microscopy and Spectrometry Laboratory, Dept. of Materials Science, École Polytechnique Federale de Lausanne, CH-1015, Lausanne, Switzerland.*

[c] *Computational Solid State Chemistry, Dept. of Chemistry, University of Bath, Claverton Down, Bath BA2 7AY, UK..*

Abstract

Transition element dopants (e.g. Y, La) are commonly used as sintering aids in polycrystalline alumina ceramics, which segregate to the grain boundaries and control the grain boundary mobility. However, due to the extremely thin (<2 nm) layer of segregated dopants, the experimental characterization of the segregated alumina grain boundaries is a complex task. Computational studies have focused only on tilt grain boundaries, which are only a small fraction in a sintered alumina sample. In this study, a quantitative characterization of the segregation of Y and La at general high angle grain boundaries in transparent alumina is carried out using a unique combination of advanced TEM and near coincidence grain boundary atomistic simulations. The result show that high angle grain boundaries may lead to enhanced grain growth in comparison to symmetric tilt twin grain boundaries due to the reduced configuration entropy for dopant segregation and higher order grain boundary complexions. On the other hand, multi-doping with different dopants was shown to be more beneficial than single doping due to its contribution in increasing the configurational entropy for segregation. The advanced TEM

analysis showed Y and La distributions and concentrations on a series of general grain boundaries in very good agreement with the atomistic simulations. This validation of atomistic modelling technique used in the current study means, since it a generic method, can be used as a predictive tool to design ceramic microstructure and properties.

1. Introduction

The use of transparent polycrystalline alumina in place of synthetic single crystals of sapphire has huge commercial promise in areas related to energy (lighting,[1] and solar energy[2,3,4]), medical implants,[5] ceramic armors[6] and, as highlighted in the use of sapphire in smart phones, as shock resistant display materials. Recent progress leading to polycrystalline aluminas with real in-line transmittances (RITs) of >70% has been made using pressure assisted sintering[7,8,9] and colloidal processing.[10,11] Light transmission properties of the polycrystalline alumina are governed by their microstructural characteristics, especially defects and grain boundaries. For higher light transmission in polycrystalline alumina needed for commercial use, grain sizes have to approach the nano regime, (<200 nm), grain alignment needs to be enhanced and pores >50nm have to be totally eliminated[11]. Currently dopants are used to control the grain size and the porosity,[7,8] the type and quantity of which are chosen empirically. However to reach transmittances approaching that of sapphire (84%) for a commercially sustainable material, in-depth investigation of the mechanisms at play in the evolution of the grain boundaries during processing of the doped powders, which control the microstructure and hence transparency, is needed.

The majority of the computational segregation studies have been done on the highly symmetrical tilt grain boundaries of varying complexities to minimize the computational cost,[12,13,14,15] which is required to simulate non symmetrical, large general grain boundaries. However, the fraction of highly symmetrical tilt grain boundaries found in the sintered alumina samples is reported to be very small.

Transmission electron microscopy studies of undoped alumina samples by Lartigue and Prister[16] showed that grain boundary misorientation is randomly distributed and the fraction of near coincidence grain boundaries is very low. It was also reported that the microstructure of alumina does not change significantly due to the Y doping,[17] however Mg doping increases the number of near coincidence grain boundaries.[18] Later these findings were confirmed by statistical determination of grain boundary misorientation using electron back scattered Kikuchi diffraction (EBKD) by Cho et al.[19] The proportion of coincidence site lattice boundaries was also reported to be very low (1-5%) in this study, which is small to have any significant effect on the properties of doped alumina. In a more recent study on transparent polycrystalline alumina, the grain boundary orientation distribution was reported to be random with no preference for low angle twin grain boundaries.[20] However, a preference for the (00.1) plane was reported in Y and La doped alumina samples.

Although it has been shown in experiments conducted on metal system that the lowest degree of segregation occurs on the grain boundaries with higher atomic densities,[21] there is not enough evidence to conclude the same in case of alumina ceramics. In addition, the variation in grain boundary volume versus concentration across different experimental studies can make them difficult to compare with one another. It has been also suggested that there is no direct relationship between three dimensional coincidence relationship and grain boundary segregation and the nature of solute and solvent atoms also needs to be taken into account in addition to the boundary characteristics.[22]

In the light of these experimental observations of mostly general grain boundaries in doped and undoped alumina, and the missing direct link between experiments and atomistic modeling, efforts are required to simulate the realistic general grain boundaries dominating in polycrystalline alumina. It will also help to understand how far the observations made on simple tilt grain boundaries in the simulations can be extended to the general grain boundaries in the real alumina samples. The breakthrough presented here is the validation of atomistic modelling predictions on doped high angle

general grain boundary structures using a combination of analytical transmission electron microscopy and large angle convergent beam electron diffraction. Instead of usually simple and computationally cheaper tilt boundaries, the atomistic simulations have been carried out on an experimentally observed general grain boundary, which allow the prediction of dopant structure at realistic boundaries and the formation of grain boundary phases (or complexions) that control the sintering and grain growth behaviour.[23]

2. Methods

2.1. Experimental Method

Transparent polycrystalline aluminas with RITs near 50% and grain sizes around 0.95 μm were prepared by Spark Plasma Sintering (SPS) codoped with 225 ppm of Y and La each.[7] 300 nm thick alumina TEM lamella were prepared using Zeiss NVision 40 CrossBeam with a focused ion beam (FIB). FEI Tecnai Osiris microscope operating at 200 kV was used for the microscopy analysis in the present work. High resolution EDX analysis was performed to quantify the dopant segregation in grain boundaries. First an individual grain boundary was tilted to be edge on and parallel to the electron beam. Then, EDX data was collected on that grain boundary with one hour acquisition time for the whole grain boundary length. Line scans were done normal to the grain boundary plane and quantified with Esprit 1.9 to give the atomic percentage of elements versus distance from grain boundary.[24] Number atomic density of alumina, and length and thickness of the grain boundary were then used to calculate the grain boundary concentration of dopant elements in the alumina sample as described in detail in the supplementary material (S1.1).

Low angle convergent beam electron diffraction (LACBED) analysis was used to identify the grain boundary orientations. To do so, first the grain boundary was tilted to be edge on and parallel to the optical axis. Then, a LACBED pattern is acquired showing the grain boundary and both adjacent

grains (figure S3 centre). Afterwards, LACBED patterns were taken from each grain while tilting the sample to get to a recognizable zone axis (Figure S3 left and right). These patterns from the starting angle, when the grain boundary is edge on, to the angle where we find a recognizable zone axis are stitched together and indexed by the JEMS software,[24] which is a tool developed at CIME, EPFL for the simulation of diffraction patterns and high resolution images. Using the first LACBED pattern from the grain boundary we were able to identify the grain boundary position in the indexed pattern and find the planes which are almost parallel to the grain boundary in each adjacent grain. Further details of the LACBED analysis can be found in the supplementary material (S1.2).

2.2. Computational Method

The Born model for solids was used to represent the energy surface of the alumina grain boundaries. The potential parameters developed by Lewis and Catlow[25] were used in the present work and the initial alumina crystal structure was taken from the work of Liu et al.[26] These potentials have been successfully used to predict α-alumina surface behaviour and compare well to ab-initio results for the Σ3 (00.1) grain boundary and the Σ7 (01.2) grain boundary, giving atomic positions within 3% of the ab-initio results.[27]

The general grain boundary simulation cell was created using the near coincidence grain boundary method as explained in detail in the supplementary material (S2.1). The general grain boundary between two grains with different miller indices can be considered as 2D hexagonal lattices for hexagonal systems. Although the crystal structure of alumina is rhombohedral, it can be approximated with a hexagonal lattice for the purpose of the current work as shown earlier by Sayle et al.[28]. A 2D coincidence site lattice was produced by rotating one lattice with respect to the other lattice about an axis perpendicular to the grain boundary plane until three lattice sites of the two grains are in common (c.f. figure S4).

Empirical force field based energy minimization was used to calculate the segregation energy of the

dopants to the general grain boundary B2 observed in the experiments (table 1). The misfit between the two grains of the grain boundary was minimized by rotating the planar lattices by 25.28° with respect to each other. The area of the resultant optimized 2D coincidence site lattice was calculated to be 5.01 nm^2.

High computational cost was the main reason behind doing the calculations on only one grain boundary. The miller indices of the other two grain boundaries (table 1) are unreasonably large, which will require larger primitive unit cell of the coincidence site lattice to minimize the misfit of two planar lattices (S2.1) and hence, will be computationally much more expensive. The simulation cells of these general grain boundaries contain more than 10000 atoms. The grain boundary region where the atoms are free to relax contains about 2500 atoms, which makes the energy minimization calculations computationally very expensive. In addition the dopant calculations were done for several dopant configurations and concentrations, increasing the number of calculations significantly for one grain boundary. It is also worth pointing out that we include a representation of the electronic polarization via the shell model, which further increases the computational cost.

First, the segregation energy of single cation sites was calculated by substituting each grain boundary Al atom with both the dopants one by one. The following expression was used to calculate the segregation energy of the dopants,

$$\Delta E_{seg}\left(N_Y + N_{La}\right) = \frac{E\left(N_Y + N_{La}\right) - E(0) - N_Y \Delta E_{bulk,Y} - N_{La}\Delta E_{bulk,La}}{\left(N_Y + N_{La}\right)} \qquad (1)$$

$\Delta E_{seg}(N)$ is the energy of segregation in a structure containing N dopant ions, $E(N)$ is the potential energy of the structure containing N dopant ions, and $\Delta E_{i,bulk}$ is the change in the energy when inserting a dopant ion i in the bulk.

The 20 highest probable single cation sites were chosen and permutated to create the configurations with higher dopant concentrations. The details of the screening method to find highest probable

configuration are explained in the supplementary material (S2.2) and in earlier work[15]. The segregation energy was calculated for the 30 highest probable configurations for each dopant concentration. Additionally, since it was impossible to explore all possible combinations of dopant concentrations, we restricted ourselves to the case of equal dopant concentration for both the dopants.

3. Results and Discussion

3.1. Grain Boundary Characterization

Figure 1 (a, b) shows an overall view of the 300 nm thick FIB prepared specimen acquired by Scanning Transmission Electron Microscopy (STEM bright field), clearly revealing the grain boundaries in a nearly equiaxed microstructure. Energy Dispersive X-ray (EDX) mapping was done on the La-L_α edge and Y-K_α edge, on the grain boundaries in the same area (figure 1c, d). EDX maps show that both the elements segregate together at all the visible grain boundaries, and there is no indication of selective segregation of the two dopants to specific grain boundaries.

High resolution EDX maps were acquired on 7 relatively straight grain boundaries (6 of them marked in figure 1a) to quantify the concentration of dopants at the grain boundaries after orienting them edge on with respect to the electron-beam (S1.1). Figure 2 shows an enlarged view of the grain boundary B6 together with the Y and La line profiles integrated over the total length of the grain boundary. The line profiles for other 6 grain boundaries are provided in the supplementary material (figure S2). The ~5 nm width of the profile (figure 2d) can be attributed to a slight residual miss tilt of the grain boundary of about 1°. The average concentration of the Y and La dopants was found to be 2.8±0.4 and 2.3±0.6 atoms/nm^2 respectively. The low value of standard deviation shows the small variation of the dopant concentration between grain boundaries, confirming the qualitative observation that the dopants segregate uniformly to the observed grain boundaries. The nominal bulk concentration corresponding to the measured grain boundary concentration can be calculated using a simple microstructural model

where the grains are approximated by truncated octahedrons (eq. 7, 8 in ref[14]) The calculated concentration comes out to be 415±85 ppm, which is in very good agreement with the nominal dopant concentration (450 ppm) of the powders.

Three grain boundaries were then characterized using large angle convergent beam electron diffraction (LACBED) to calculate their orientation and grain boundary planes (table 1). LACBED can identify the plane of the grain boundary with a high accuracy (less than 1°) without relying on the precision of the goniometer as would be the case with selected area diffraction patterns. The three investigated grain boundaries were all random high angle grain boundaries.

3.2. Segregation Energy Calculations

Grain boundary B2 (table 1) was chosen in the present work for the atomistic modelling of Y and La-dopant segregation in a Y-La codoped samples for its relative simplicity in comparison to other two grain boundaries. One of the planes in grain boundary B2 is parallel to (00.1), which was found preferably in La and Y-doped alumina samples in our earlier EBSD study[20]. Therefore, it will be provide further insights into the experimental findings.

3.2.1. Single Dopants

The ΔE_{seg} for single cation sites in 2 Å region on both sides of the grain boundary varies from -3.3 to 15.7 eV/atom for Y and La (Figure 3b). ΔE_{seg} is more negative for La in comparison to Y because there is a stronger driving force for the segregation of La due to the higher bulk elastic strain caused by larger La ions. However, only ~25% of the sites have negative ΔE_{seg}, hence are energetically favourable for segregation, as can be observed in figure 3b. This is in contrast to the depth profile observed in the case of simulation of Y or La segregation on tilt grain boundaries, where almost all the cation sites were found to be energetically favourable for segregation,[27] this indicates a lower configurational entropy for the case of general grain boundary in comparison to tilt grain boundary. In an STEM study of a $\sum 13$ grain boundary,[29] bi-crystal tilt boundary, Shibata et al also showed that the

Y-atoms selectively occupy only specific atomic sites on the grain boundary, which is in agreement with our current calculations on a near coincidence grain boundary.

The majority of the energetically favourable cation sites were observed to be on the lower index plane (00.1) of the grain boundary (figure 3a). This can be attributed to the lower atomic density of the (00.1) plane providing extra space for larger dopants causing lower structural strain due to the segregation. Lartigue et al.[21,30] also reported a reduced segregation on the grain boundaries, whose plane is parallel to one of the higher atomic density planes in both the grains. It can also be observed (top panel, figure 3) that Y and La occupy different sites at the grain boundaries, i.e. there are two different sets of favourable sites for two dopants. Therefore, higher dopant concentration can be accommodated at the grain boundaries for the case of codoping in comparison to single doping due to increased number of favourable sites, which leads to enhanced solute drag effect. In addition, the configurational entropy is also increased in case of codoping due to the higher number of choices available for the segregation of dopants, thereby making the free energy of segregation more negative.

Therefore, on the one hand configurational entropy of segregation decreases on a general grain boundary due to the reduced number of energetically favourable cation sites, but on the other hand it increases for the codoping due to two mutually exclusive sets of cationic sites present for the segregation of two different dopants.

3.2.2. Codoping

Although only a certain number of cation sites (25%) are energetically favourable for the segregation, ΔE_{seg} for all the calculated dopant concentrations and configurations was found to be negative (figure 3b) making segregation energetically favourable. Therefore, the number of favourable grain boundary cation sites is sufficient to accommodate the dopant ions at the experimentally observed concentrations (4-5 atoms/nm^2).

Figure 4 shows the atomistic structures of Y-La codoped grain boundary at varying dopant

concentrations. Codoping is seen to be energetically favourable and both dopants should be found at the grain boundary as seen experimentally. i.e. there is no preference for one or other dopant at this general grain boundary. Distinct grain boundary phases can be observed at different dopant concentrations (figure 4), which will determine the mobility of the grain boundary. These grain boundary phases are thermodynamically stable at the grain boundary but do not exist as the bulk phase, and are also termed as grain boundary complexions.[31,32] The dopants are adsorbed in a bilayer complexion at the grain boundary for all the calculated concentrations. This is in contrast to the simulated tilt grain boundaries, where the dopants segregate in a monolayer complexion at lower concentrations as seen in a (11.1) Y-La codoped grain boundary (supplementary material S2.3, figure S6). The higher order bilayer complexion is formed in the general grain boundary at the same dopant concentrations. In an earlier analytical modelling study[33], it was also reported that lower order complexions exist over shorter concentration ranges on high energy general grain boundaries than lower energy symmetric tilt grain boundaries, again coherent with our simulations. Therefore according to the grain boundary complexion theory[23], it is expected that the presence of high angle general grain boundaries will lead to the higher grain boundary mobility and hence enhanced grain growth in comparison to symmetric tilt grain boundaries.

4. Conclusions

In this study, TEM-EDX analysis of the La-Y codoped polycrystalline transparent alumina sample showed that the dopants segregate together to the general high angle grain boundaries, identified in the microstructure characterized using low angle convergent beam electron diffraction (LACBED) analysis. One of the experimentally observed high angle general grain boundaries was simulated for the first time using near coincidence grain boundary approach, where segregation of both dopants together was predicted in line with the experimental observations. Segregation calculations showed

that the general high angle grain boundaries behave very differently to the often simulated/studied tilt grain boundaries: Only a certain fraction of grain boundary cation sites (about ¼) were found to be energetically favourable for the segregation and higher order grain boundary complexions were predicted to be more probable at the general grain boundaries when compared to tilt grain boundaries. It was also shown that the beneficial effects of codoping over single doping stem from the increased configuration entropy of the segregation due to the higher number of energetically favourable sites available for two dopants, the different dopants occupy different sites. The concentration at the grain boundaries measured experimentally and from the simulation matched very well, validating the general simulation method.

The current findings suggest that by increasing the fraction of symmetric tilt grain boundaries and by using multiple dopants (codoping or triple-doping) better grain growth reduction and hence, higher transparency in polycrystalline alumina can be achieved. The power of the analytical TEM and electron diffraction approach combined with atomistic scale simulation has given deep insight into general doped grain boundary behaviour in alumina, but the approach is generic and can be applied to other ceramic systems. This type of knowledge can lead us towards atomistically engineered grain boundaries and enhanced ceramic and device properties, in particular by defining concentrations that produce specific grain boundary phases (or complexions) and hence their behaviour.

Acknowledgements

The authors would like to thank the Swiss National Science Foundation SNF project No. 200020_144499 for the financial support for the current work.

References

[1] G.C. Wei, “Transparent ceramic lamp envelope materials,” *J. Phys. Appl. Phys.*, **38** [17] 3057–3065 (2005).

[2] J. Peet, J.Y. Kim, N.E. Coates, W.L. Ma, D. Moses, A.J. Heeger, and G.C. Bazan, "Efficiency enhancement in low-bandgap polymer solar cells by processing with alkane dithiols," *Nat. Mater.*, **6** [7] 497–500 (2007).

[3] D. Chen, Y. Wang, Y. Yu, P. Huang, and F. Weng, "Near-infrared quantum cutting in transparent nanostructured glass ceramics," *Opt. Lett.*, **33** [16] 1884–1886 (2008).

[4] M. Liu, Y. Lu, Z.B. Xie, and G.M. Chow, "Enhancing near-infrared solar cell response using upconverting transparentceramics," *Sol. Energy Mater. Sol. Cells*, **95** [2] 800–803 (2011).

[5] J. Chevalier and L. Gremillard, "Ceramics for medical applications: A picture for the next 20 years," *J. Eur. Ceram. Soc.*, **29** [7] 1245–1255 (2009).

[6] A. Krell, J. Klimke, and T. Hutzler, "Advanced spinel and sub-[mu]m Al2O3 for transparent armour applications," *J. Eur. Ceram. Soc.*, **29** [2] 275–281 (2009).

[7] M. Stuer, Z. Zhao, U. Aschauer, and P. Bowen, "Transparent polycrystalline alumina using spark plasma sintering: Effect of Mg, Y and La doping," *J. Eur. Ceram. Soc.*, **30** [6] 1335–1343 (2010).

[8] N. Roussel, L. Lallemant, J.-Y. Chane-Ching, S. Guillemet-Fristch, B. Durand, V. Garnier, G. Bonnefont, G. Fantozzi, *et al.*, "Highly Dense, Transparent α-Al2O3 Ceramics From Ultrafine Nanoparticles Via a Standard SPS Sintering," *J. Am. Ceram. Soc.*, **96** [4] 1039–1042 (2013).

[9] M. Trunec, K. Maca, and R. Chmelik, "Polycrystalline alumina ceramics doped with nanoparticles for increased transparency," *J. Eur. Ceram. Soc.*, **35** [3] 1001–1009 (2015).

[10] A. Krell, T. Hutzler, and J. Klimke, "Transmission physics and consequences for materials selection, manufacturing, and applications," *J. Eur. Ceram. Soc.*, **29** [2] 207–221 (2009).

[11] M. Stuer, P. Bowen, M. Cantoni, C. Pecharroman, and Z. Zhao, "Nanopore Characterization and Optical Modeling of Transparent Polycrystalline Alumina," *Adv. Funct. Mater.*, **22** [11] 2303–2309 (2012).

[12] J.P. Buban, K. Matsunaga, J. Chen, N. Shibata, W.Y. Ching, T. Yamamoto, and Y. Ikuhara, "Grain Boundary Strengthening in Alumina by Rare Earth Impurities," *Science,* **311** [5758] 212 –215 (2006).

[13] C. Elsässer and T. Elsässer, "Codoping and Grain-Boundary Cosegregation of Substitutional Cations in α-Al_2O_3: A Density-Functional-Theory Study," *J. Am. Ceram. Soc.,* **88** [1] 1–14 (2005).

[14] S. Galmarini, U. Aschauer, A. Tewari, Y. Aman, C. Van Gestel, and P. Bowen, "Atomistic modeling of dopant segregation in α-alumina ceramics: Coverage dependent energy of segregation and nominal dopant solubility," *J. Eur. Ceram. Soc.,* **31** [15] 2839–2852 (2011).

[15] A. Tewari, S. Galmarini, M. Stuer, and P. Bowen, "Atomistic modeling of the effect of codoping on the atomistic structure of interfaces in α-alumina," *J. Eur. Ceram. Soc.,* **32** [11] 2935–2948 (2012).

[16] S. Lartigue and L. Priester, "Influence of doping elements on the grain boundary characteristics in alumina," *J. Phys. Colloq.,* **49** [C5] C5–451–C5–456 (1988).

[17] D. Bouchet, F. Dupau, and S. Lartigue-Korinek, "Structure and chemistry of grain boundaries in yttria doped aluminas," *Microsc. Microanal. Microstruct.,* **4** [6] 13 pages (1993).

[18] S. Lartigue and L. Priester, "Grain Boundaries in Fine-Grained Magnesium-Doped Aluminas," *J. Am. Ceram. Soc.,* **71** [6] 430–437 (1988).

[19] J. Cho, H.M. Chan, M.P. Harmer, and J.M. Rickman, "Influence of yttrium doping on grain misorientation in aluminum oxide," *J. Am. Ceram. Soc.,* **81** [11] 3001–3004 (1998).

[20] S.A. Bojarski, M. Stuer, Z. Zhao, P. Bowen, and G.S. Rohrer, "Influence of Y and La Additions on Grain Growth and the Grain-Boundary Character Distribution of Alumina," *J. Am. Ceram. Soc.,* **97** [2] 620–630 (2013).

[21] S. Lartigue-Korinek, C. Carry, and L. Priester, "Multiscale aspects of the influence of yttrium on microstructure, sintering and creep of alumina," *J. Eur. Ceram. Soc.,* **22** [9-10] 1525–1541 (2002).

[22] A.P. Sutton and R.W. Balluffi, *Interfaces in Crystalline Materials*. OUP Oxford, 1995.

[23] S.J. Dillon and M.P. Harmer, "Demystifying the role of sintering additives with 'complexion,'" *J. Eur. Ceram. Soc.*, **28** [7] 1485–1493 (2008).

[24] P.A. Stadelmann, "EMS - a software package for electron diffraction analysis and HREM image simulation in materials science," *Ultramicroscopy*, **21** [2] 131–145 (1987).

[25] G.V. Lewis and C.R.A. Catlow, "Potential models for ionic oxides," *J. Phys. C Solid State Phys.*, **18** [6] 1149–1161 (1985).

[26] R.S. Liu, W.C. Shi, Y.C. Cheng, and C.Y. Huang, "Crystal structures and peculiar magnetic properties of α- And γ-Al2O3 powders," *Mod. Phys. Lett. B*, **11** [26-27] 1169–1174 (1997).

[27] S. Galmarini, U. Aschauer, P. Bowen, and S.C. Parker, "Atomistic Simulation of Y-Doped α-Alumina Interfaces," *J. Am. Ceram. Soc.*, **91** [11] 3643–3651 (2008).

[28] T.X.T. Sayle, C.R.A. Catlow, D.C. Sayle, S.C. Parker, and J.H. Harding, "Computer simulation of thin film heteroepitaxial ceramic interfaces using a near-coincidence-site lattice theory," *Philos. Mag. A*, **68** [3] 565–573 (1993).

[29] N. Shibata, S.D. Findlay, S. Azuma, T. Mizoguchi, T. Yamamoto, and Y. Ikuhara, "Atomic-scale imaging of individual dopant atoms in a buried interface," *Nat. Mater.*, **8** [8] 654–658 (2009).

[30] W. Swiatnicki, S. Lartigue-Korinek, and J.Y. Laval, "Grain boundary structure and intergranular segregation in Al2O3," *Acta Metall. Mater.*, **43** [2] 795–805 (1995).

[31] P.R. Cantwell, M. Tang, S.J. Dillon, J. Luo, G.S. Rohrer, and M.P. Harmer, "Grain boundary complexions," *Acta Mater.*, **62** 1–48 (2014).

[32] T. Frolov, D.L. Olmsted, M. Asta, and Y. Mishin, "Structural phase transformations in metallic grain boundaries," *Nat. Commun.*, **4** 1899 (2013).

[33] J. Luo, "Grain boundary complexions: The interplay of premelting, prewetting, and multilayer adsorption," *Appl. Phys. Lett.*, **95** [7] 071911 (2009).

Table 1. Grain boundary misorientation angles and grain boundary planes determined using the Large Angle Convergent Beam Electron Diffraction method for Y, La codoped sintered alumina.

GB[a] #	**Misorientation**	**GB Planes**
B1	55°	$(\bar{4}\bar{1}.\bar{2})$ || (01.1)
B2	46°	(00.1) || (01.3)
B3	148°	(00.1) || $(\bar{1}1.\bar{5})$

[a] GB: grain boundary.

List of Figures

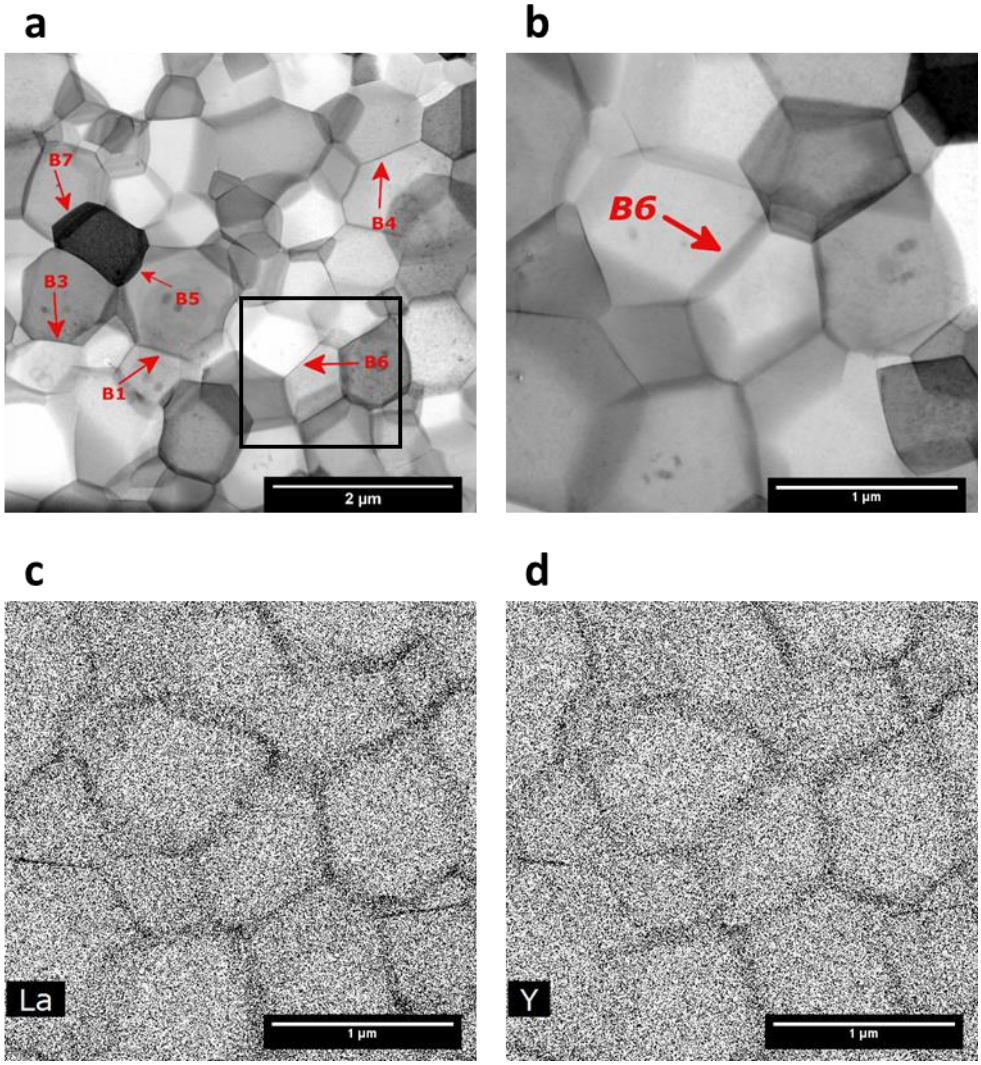

Fig.1 General view of the sintered alumina specimen with marked grain boundaries. (a) STEM bright filed image. (b) Enlarged view (of box in a), (c) La and (d) Y EDX maps for the enlarged view.

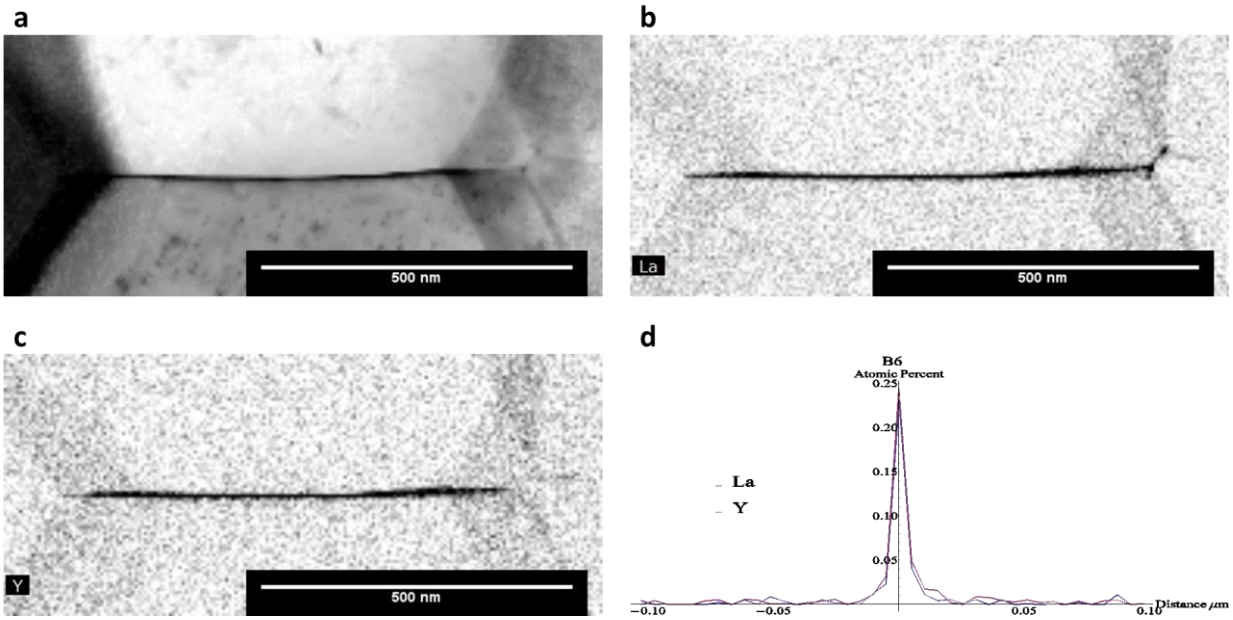

Fig.2 Chemical analysis of a grain boundary B6. (a) STEM - bright field image, (b) La and (c) Y high resolution EDX maps integrated over 60 minutes. (d) Y and La concentration across the grain boundary (at 0 μm) averaged over the whole length of the grain boundary for the doped sintered alumina.

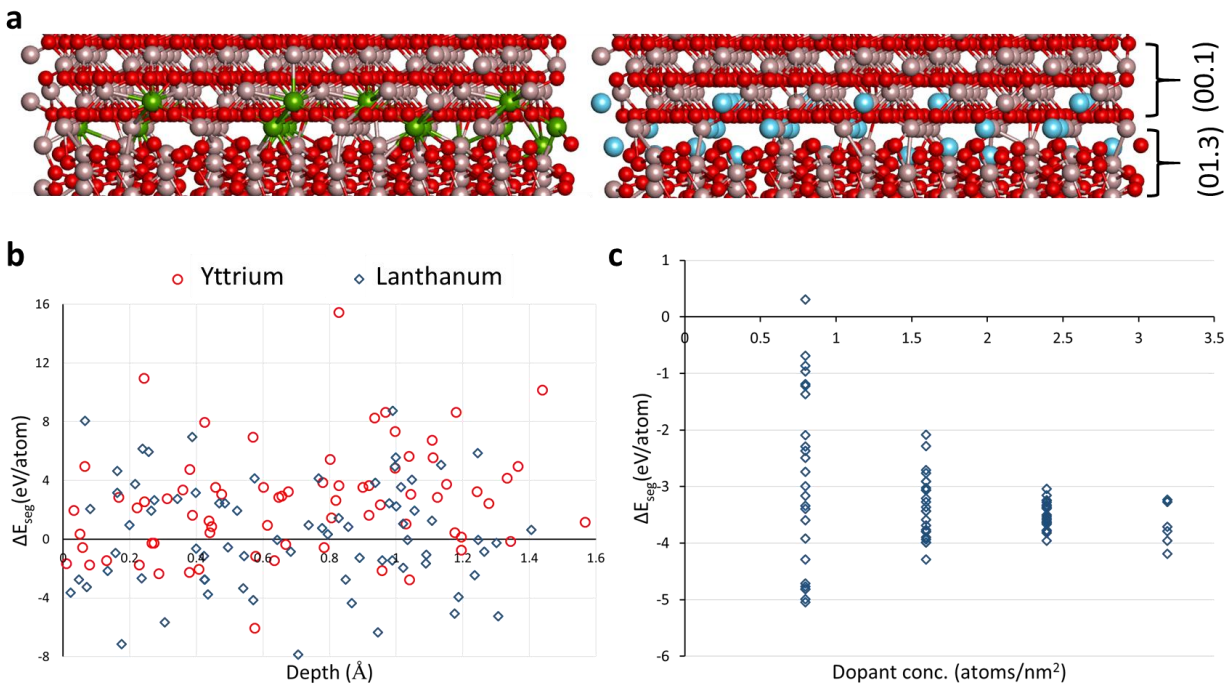

Fig.3 Segregation energies for Y and La dopants. (a) Energetically favourable cation sites for Y (green) and La (light blue) segregation at the alumina general grain boundary. (b) Segregation energy of the single cation sites as a function of distance from the grain boundary. (c) Codoping segregation energies for different configurations as a function of total dopant concentration (La+Y).

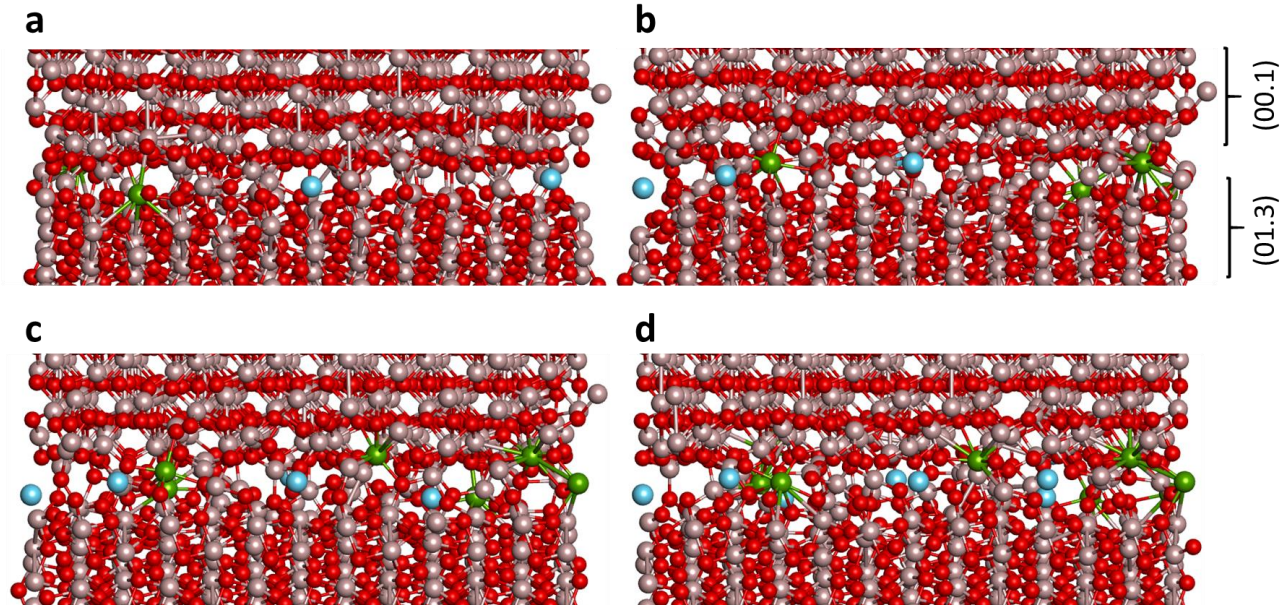

Fig.4 Atomistic structure of codoped grain boundary with increasing dopant concentration. Dopants are accommodated in bilayer complexion even at lower dopant concentrations. (a) 0.8 at./nm^2, (b) 1.6 at./nm^2, (c) 2.4 at./nm^2, and (d) 3.2 at./nm^2. All the atomistic structures are seen parallel to the grain boundary plane. (Y: green, La: light blue, Al: pink, O: red)